Sn Substitution by Ge: Strategies to Overcome the Open-Circuit Voltage Deficit of Kesterite Solar Cells

Peer-reviewed author version

Choubrac, Leo; Baer, Marcus; Kozina, Xeniya; Felix, Roberto; Wilks, Regan G.; BRAMMERTZ, Guy; Levcenko, Sergiu; Arzel, Ludovic; Barreau, Nicolas; Harel, Sylvie; MEURIS, Marc & VERMANG, Bart (2020) Sn Substitution by Ge: Strategies to Overcome the Open-Circuit Voltage Deficit of Kesterite Solar Cells. In: ACS APPLIED ENERGY MATERIALS, 3 (6) , p. 5830 -5839.

DOI: 10.1021/acsaem.0c00763
Handle: http://hdl.handle.net/1942/31890

Sn substitution by Ge: Strategies to overcome the open circuit voltage deficit of kesterite solar cells

Leo Choubrac(1,2), Marcus Bär(3,4,5,6), Xeniya Kozina(3), Roberto Félix(3), Regan G. Wilks(3,4), Guy Brammertz(7,8,9), Sergej Levcenko(2), Ludovic Arzel(1), Nicolas Barreau(1), Sylvie Harel(1), Marc Meuris(7,8,9), Bart Vermang(7,8,9).*

(1) Institut des Matériaux Jean Rouxel (IMN) - UMR6502, CNRS, Université de Nantes, 44300 Nantes, France

(2) Helmholtz-Zentrum Berlin für Materialien und Energie GmbH, Department Structure and Dynamics of Energy Materials, Hahn-Meitner-Platz 1, D-14109 Berlin, Germany

(3) Department of Interface Design, Helmholtz-Zentrum Berlin für Materialien und Energie GmbH (HZB), Berlin, Germany

(4) Energy Materials In-Situ Laboratory Berlin (EMIL), Helmholtz-Zentrum Berlin für Materialien und Energie GmbH, Berlin, Germany

(5) Helmholtz-Institute Erlangen-Nürnberg for Renewable Energy (HI ERN), Berlin, Germany

(6) Department of Chemistry and Pharmacy, Friedrich-Alexander-Universität (FAU) Erlangen-Nürnberg, Erlangen, Germany

(7) IMEC Division IMOMEC – Partner in Solliance, Wetenschapspark 1, 3590 Diepenbeek, Belgium

(8) Hasselt University – Partner in Solliance, Martelarenlaan 42, 3500 Hasselt, Belgium

(9) EnergyVille, Thorpark 8320, 3600 Genk, Belgium

KEYWORDS: kesterite, CZGSe, VOC, germanium, high voltage

ABSTRACT

Current state-of-the-art $Cu_2ZnSn(S,Se)_4$ kesterite solar cells are limited by low open circuit voltages (V_{OC}). In order to evaluate to what extent the substitution of Sn by Ge is able to result in higher V_{OC} values, this article focuses on $Cu_2ZnGeSe_4$ "CZGSe" devices. To reveal their full potential, different strategies are explored that in particular aim at the optimization of the CZGSe/buffer heterojunction. Employing hard x-ray photoelectron spectroscopy, here is evidenced that only a combination of different surface treatments is able to remove all detrimental secondary phases. Further improvements are achieved by establishing a solar cell heat treatment in air. A systematic study of the impact of different annealing temperatures and durations determines the best heat treatment parameters to be 60 min at 200 °C. Also Zn(O,S,OH) as a more transparent alternative to the heavy-metal compound CdS buffer layer has been realized. Combining all of the strategies, solar cells with 8.5% and 7.5% total area efficiency have been prepared which consists in record for Sn-free kesterite solar cells and any kesterite solar cell with a Zn(O,S,OH) buffer, respectively. Beyond those records, this work clearly confirms the emerging trend that Ge for Sn substitution is a successful strategy to improve the V_{OC} of kesterite solar cells.

1. Introduction

$Cu_2ZnSn(S,Se)_4$ "CZTSSe" kesterite-based materials have gained significant interest in the thin-film solar cell community thanks to their properties. CZTSSe consists of non-toxic and earth abundant elements, by changing the S/Se ratio the bandgap can easily be tuned, and highest solar cell efficiencies have been reported for solution-processed kesterites – allowing for cheaper and faster upscalable production in comparison to vacuum-based processing methods. A fast improvement of device performance was achieved during the 2008-2012 period using conventional Sn-based CZTSSe kesterites as thin-film solar cell absorbers,[1] resulting in a certified record power conversion efficiency of 12.6%.[2] Recently, several teams demonstrated efficiencies higher than 10% using diverse deposition methods and different absorber compositions.[3,4] Despite this diversity, the common parameter limiting the performance in all of these kesterite-based solar cells is the low open circuit voltage (V_{OC}), especially in comparison to the maximum possible V_{OC} value governed by the Shockley-Queisser radiative limit ($V_{OC,SQ}$).[5] In particular, Bourdais *et al.* pointed out recently that, regardless of their bandgap, all Sn-kesterite based devices fail to exceed 60% of $V_{OC,SQ}$;[6,7] which contrasts corresponding short circuit current densities (J_{SC}) and fill factors (FF) reaching values higher than 80% of their respectively calculated limits. Consequently, a V_{OC} improvement appears to be a prerequisite to bring kesterite-based solar cells on par with their chalcopyrite, CdTe, or halide perovskite counterparts making large-scale industrial production economical feasible.

Amongst the numerous strategies applied to overcome this limitation, many studies were devoted to cationic alloying (Li or Ag for Cu,[8,9] Cd, Ba, Fe, Co, Ni or Mn for Zn,[10–13] Ge for Sn[14]). To date, the only noticeable V_{OC} improvement results from the (partial) substitution of Sn by Ge. For Ge/(Ge+Sn) ratios between 20 and 30% the best results are reported, however, for higher

substitution ratios significant losses are observed.[14–16] As a result, the highest efficiencies reported for completely Ge-substituted kesterite solar cells are 7.6%[17] and 6.0%[18] for $Cu_2ZnGeSe_4$ "CZGSe" and $Cu_2ZnGe(S,Se)_4$ "CZGSSe" compounds, respectively, with V_{OC} values limited to 48 % and 51 % of the respective theoretical maximum value.

The present paper aims at evaluating the full potential of substituting Sn by Ge in kesterite-based solar cells with a particular focus on improving V_{OC}. Therefore, Sn-free CZGSe absorbers were used in this investigation to test and implement diverse optimization strategies to increase performance.

In particular, we aim at minimizing the charge carrier recombination at the absorber/buffer pn-heterojunction following three approaches:

1- Develop and employ a CZGSe surface treatment to remove undesired and detrimental secondary phases.

2- Introduce a heat treatment of the complete solar cell layer stack to allow for/enhance (beneficial) chemical interaction and/or interdiffusion at the absorber/buffer/ window interfaces.

3- Application of an alternative buffer layer, namely Zn(O,S,OH) instead of CdS as already reported by Schnabel et al;[18] combining a Cd-free wide bandgap window (resulting in higher transparency) with the possibility to improve the energy level alignment at the CZGSe/buffer interface.

As major new result of the combination of these approaches, the V_{OC} of respectively optimized solar cells devices value reaches 65% of the theoretical limit, demonstrating the relevance and effectiveness of the Sn substitution by Ge and the need for additional optimization strategies. The

origin of the outstanding V_{OC} is discussed based on available literature and new results. Ultimately, we report on two new records in efficiency: 8.5% for a CZGSe/CdS based device (record efficiency for this absorber compoisition); and 7.5% for a CZGSe/ Zn(O,S,OH) based device (record efficiency for this buffer and any kesterite absorber, including CZTSSe).[19]

2. Materials and Methods

Materials Preparation:

CZGSe absorbers were prepared according to Brammertz et al[20] by annealing e-beam deposited stacks of Ge/Zn/Cu elemental layers under H_2Se gas flow. Soda-lime Glass (SLG) covered with a 120nm Si(O,N) alkali-diffusion barrier and a Mo layer acting as back contact were used as substrate; no alkali or additional dopant was deliberately incorporated at any stage of the preparation. Thus the CZGSe absorbers were prepared according to the same recipe as used for the previous record solar cells.[17]

Some of the absorbers underwent chemical treatments prior to buffer layer deposition, namely etching in HCl and/or passivation in ammonium sulfide ($(NH_4)_2S$) solutions. As already reported,[21] the etching treatment consisted of dipping the absorber in a hot (80°C) aqueous solution of HCl (12 wt%) for 20 min. The ammonium sulfide passivation treatment was performed by dipping the absorber in an aqueous solution of $(NH_4)_2S$ (20 wt%) at room temperature for 40 min. Depending on the applied treatment, absorbers as well as related solar cells are labeled “AG” when as-grown CZGSe absorbers (i.e., absorbers that have not been chemically treated) are considered; “E” when the CZGSe has only been etched in hot HCl; and “EP” when absorbers have been etched in hot HCl and subsequently passivated in an ammonium sulfide solution.

The optimization of the chemical bath deposition (CBD) process for the CdS buffer layer employed on CZGSe is reported elsewhere.[17] According to this previous work, the optimal CBD conditions for the CdS buffer for this absorber and setup are 6 min in a bath heated at 52 °C, which were also applied for the CdS buffer layers used in this study.

On some of the absorbers a CBD-Zn(O,S,OH) buffer layer was applied instead of the CdS. In this case, the aqueous bath temperature was 80 °C; the reactants were zinc sulfate [$ZnSO_4 \cdot 7H_2O$, 0.15 M, Alfa Aesar, ACS 99.0-103%] and thiourea [0.55 M, Alfa Aesar, ACS 99% min] dissolved in ultrapure water. Aqueous ammonia [4.2 M, Carlo ERBA Reagants SAS is added before absorbers are dipped in the reaction bath (190 ml) for 20 min.

After each chemical treatment as well as buffer layer deposition, the samples are rinsed in diluted (1 M) aqueous ammonia.

CZGSe/buffer stacks were completed to solar cell devices by RF-sputtered ZnO (≈80 nm) and Al-doped ZnO (≈200 nm) layers. Last, Ni/Al contact grids were applied by e-beam evaporation. Before electrical characterization, cells 0.25 and 0.5 cm^2 in size were mechanically separated. For a few solar cells 120 nm MgF_2 was deposited by thermal evaporation on top as antireflective coating (ARC).

Characterization and Methods: The device parameters were derived from I(V) measurements using a solar simulator (ORIEL) equipped of an AM1.5 filter at 1000 W/m^2 (calibrated using a Si reference cell) and 25°C cell temperature.

External quantum efficiency (EQE) measurement were performed using a custom-built setup that also allows for bias dependent measurements. The recorded EQE was calibrated using the

quantum efficiency of Si and InGaAs reference cells. Active area J_{SC} were calculated by integrating the product of the measured EQE with the AM1.5G solar spectrum, total area J_{SC} were then calculated from the total and active area determined by means of an optical microscope. To quantify the band tailing, the Urbach energy (E_U) was estimated by the fitting of a plot of ln[−ln(1 – EQE)] vs energy.[22]

The heat treatments (HT) of the full solar cell layer stack were performed in the dark at 200°C in ambient atmosphere. After HT, the samples were left to cool down rather slowly (without active cooling): 1 h to reach 120°C, then 8 h to reach room temperature. This procedure is motivated by previous investigations showing that in the case of Sn-kesterite material, HT within this temperature range has an impact on the structural disorder in the Cu-Zn plane,[23] affecting intrinsic material properties, such as the optical bandgap energy, E_g.[24] Additional details on this phenomenon are provided in the section 1 of the Supporting Information (in conjunction with Figure S1). In the present work, all absorbers have a bandgap of (1.40±0.05) eV and considered to have a low Cu-Zn disorder.

At HZB AG, E, and EP absorbers were characterized by hard x-ray photoelectron spectroscopy (HAXPES). To minimize surface contamination via air exposure the samples prepared at Imec (and surface treated at IMN) were sealed in inert gas for the transportation. After arrival at HZB, the samples were transferred into the ultra-high vacuum (UHV, base pressure $<5\times10^{-9}$mbar) analysis system by means of N_2-filled glove bag attached to the system's load-lock chamber. The HAXPES measurements were performed at the HiKE endstation[25] located at the KMC-1 beamline[26] of HZB's BESSY-II synchrotron facility using a photon energy of 2.1 keV. The energy distribution of the photoemitted electrons was analyzed using a hemispherical analyzer (VG Scienta R4000). The total energy resolution was approximately 260 meV, as verified by Fermi

level (E_F) spectra of a clean Au foil, which was set to 0 eV to calibrate the binding energy scale. The measurements were performed at 300 K in the grazing incidence geometry with an x-ray beam take-off-angle of approximately 5° and a fixed angle of 90° between the spectrometer and the photon beam assuring maximal detection efficiency. The vertical spot size on the sample is approximately 100 μm, while in horizontal direction, along the entrance slit of the analyzer, the spot was stretched to approximately 7 mm, i.e. over the whole sample. The spectra were collected using a pass energy of 100 eV. For detailed analysis the Se 3d and Ge 3d shallow core level spin-orbit split doublets were fitted by two Voigt profiles considering the (2j+1) multiplicity rule and a doublet separation of 0.85 and 0.57 eV,[27] respectively. The spectra for all samples were fitted simultaneously with coupled Lorentzian and Gaussian width and a linear background. The position of the valence band maximum (VBM) with respect to the Fermi level (E_F) was derived by linear approximation of the leading VB edge to the background.

Photoluminescence (PL) spectra were acquired with a Hamamatsu C12132 time-resolved photoluminescence tool. The sample was illuminated on a 3 mm² area with a 15 kHz pulsed YAG laser at 532 nm with an average power of 1 mW. PLmax refers to the energy at which the PL emission is maximum.

Recently, several authors[6,14] suggested $V_{OC}/V_{OC,SQ}$ as the most appropriate metric to discuss and compare kesterite-based V_{OC} values when absorbers with various bandgaps are considered. Comparing the absolute V_{OC} deficit ($\Delta V_{OC}=(E_g/q)-V_{OC}$) from devices made from absorbers with significantly different bandgap can be misleading and often result in biased conclusions which could be avoided by referring to $V_{OC}/V_{OC,SQ}$. For these considerations, $V_{OC,SQ}$ values computed by S. Ruhle[28] have been used (for a single-junction solar cell at a temperature of 25 °C illuminated with AM1.5G (ASTM G173-03) according to Schockley-Queisser considering radiative emission

only from the front side due to the location of perfect reflector at the rear side). For Table II, $J_{SC}/J_{SC,SQ}$ and FF/ FF_{SQ} have been calculated accordingly using $J_{SC,SQ}$ and FF_{SQ} values from the same source.

Various methods can be used to determine the bandgap of the absorber. Carron *et al*[29] recently reported their recommendations and criteria of choice; their main conclusion is that two EQE-based methods can be implemented: taking the derivative of EQE *vs* E or using $(E \cdot EQE)^2$ *vs* E (with E being the photon energy). In our study, E_g values are derived using both methods (see Supporting Information, Figure S2). However, due to the presence of interference fringes in the EQE spectra (which makes it difficult to determine the derivative extrema) the $(E \cdot EQE)^2$ approach turned out to be more robust. By recording and evaluating EQE spectra measured at different voltage biases, it was ensured that the extracted E_g values were not influenced by low charge carrier collection lengths (see discussion and figure in Supporting Information Section S2).

The extrapolation of qV_{OC} (T) values to 0 K yields the activation energy of the dominating recombination process (E_a).[30] Following Siebentritt *et al*,[31] the influence of interface recombination is here discussed by comparing E_a (derived based on V_{OC} values measured under AM 1.5G at varying cell temperature as controlled by the Peltier element of the cooling stage, see Supporting Information for more details) with the energy of the radiative recombination in the bulk (E_{RR}, determined by linear extrapolation of the EQE – see Figure S2 in Supporting Information for more details).

3. Results and Discussion

3.1. Hydrochloric acid etching and ammonium sulfide passivation

3.1.1. Effects on devices

The investigated CZGSe absorbers were prepared following the same procedure as detailed in Choubrac *et al*[17] and Vermang *et al*[21] and are therefore partly covered with a ZnSe secondary surface phase of a thickness of several tens of nanometers. To remove this phase, we employed the recently developed hot HCl treatment during which the ZnSe is etched off the absorber surface.[32] As a result, solar cells prepared from HCl etched CZGSe absorbers show a significantly improved V_{OC} compared to those prepared from as-grown reference absorbers (**Figure 1a**). This suggests that the ZnSe surface phase removal lowers interface recombination. However, as depicted in **Figure 1b** and **Figure 1c**, the hot HCl treatment also results in strongly reduced FF values and (based on the suppressed EQE in the long wavelength region) a severely deteriorated charge carrier effective collection length (thus limiting J_{SC}). In addition, those losses are accompanied by a significant decrease of the photoluminescence (PL) intensity (see Figure S4 in Supporting Information).

After HCl etching, we investigate the effect of an ammonium sulfide ($(NH_4)_2S$) treatment, already reported to passivate the surface of kesterite and chalcopyrite absorbers.[33,34] Solar cells prepared from EP-CZGSe absorbers successfully combine an improved V_{OC} (as also observed for the E-CZGSe absorbers) with reasonable FF and collection length (Figure 1). Furthermore, the initial PL intensity is restored (Figure S4 in Supporting Information). It is not clear if the observed changes in the PL intensity are related to bulk (carriers lifetime, doping) or surface properties of

the absorber, but a higher PL intensity is preferred as it indicates a larger quasi Fermi level splitting.[35]

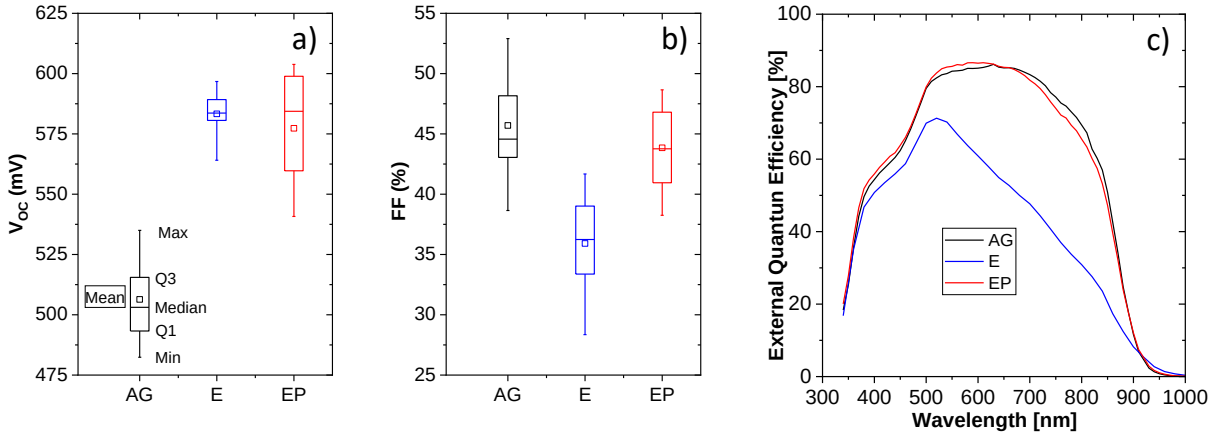

Figure 1. Electrical parameters of solar cells prepared with AG, E and EP absorbers with CdS buffer layer and without HT
a and b (Left and center): Boxplots of V_{OC} and FF (10 cells per box)
c (Right): EQE of the representative solar cell

3.1.2. Hard X-ray Photoelectron Spectroscopy

To get insight on why the different chemical treatments impact solar cell performance very differently, we studied their impact on the chemical and electronic surface structure of the CZGSe absorbers. The HAXPES spectrum of the shallow core level region of AG-, E, and EP-CZGSe absorbers show all the expected absorber related photoemission lines (Zn 3p, Cu 3p, Se 3d, Ge 3d, and Zn 3d, see Figure S5 in Supporting Information). It can be observed that while the Se 3d intensity stays (within approximately ±20%) constant independent of chemical treatment, the Zn-related lines drop to ≈ 20% intensity after HCl etching and increase again by ≈ 70% after additional passivation treatment. At the same time an HCl-etch – induced increase of the Cu 3p intensity by approximately 140% with another increase by ≈ 20% after passivation can be seen. Similarly (but

to a greater extent) the intensity of the Ge 3d is enhanced by ≈ 75% after HCl etching and by another ≈ 75% after passivation. These varying line intensities indicate a change of surface composition due to the different chemical treatments. The intensity decrease of the Zn-related lines and the increase of all other shallow core levels, which is observed comparing the AG-CZGSe and E-CZGSe absorbers, is in agreement with the removal of a ZnSe secondary phase from the CZGSe surface due to HCl etching, corroborating earlier reports.[21] For a more detailed understanding on what happens upon the different chemical treatments, we consult the detail spectra of the Se 3d and Ge 3d shallow core level next. **Figure 2a** shows the detailed fit analysis of the Se 3d levels. For the AG and E-CZGSe absorbers, two doublets are required for a reasonable fit, while for the EP-CZGSe sample one spin-orbit split Se 3d doublet is sufficient. The Se $3d_{5/2}$ main contribution (M) of the AG-CZGSe can be found at a binding energy, BE, of (54.0 ± 0.1) eV. Its secondary contribution (S) is at a BE of (54.6 ± 0.1) eV. After HCl etching both contributions are shifted to higher BE values of 54.2 and 55.2 (± 0.1) eV, respectively. At the same time the intensity ratio of the main and secondary contribution to the Se 3d line increases from $S/M^{AG} = 0.20$ to $S/M^{E} = 0.32$. Based on the comparison with reported Se $3d_{5/2}$ BE values (see top of Figure 2a) together with the significant decrease of the Zn-related shallow core level lines (see Figure S5 in Supporting Information) and the related increase of the Cu 3p and Ge 3d line, we attribute the main contribution to the Se 3d line of the AG-CZGSe to selenium in a ZnSe environment (see Supporting Information for details). Note that the indicated Se $3d_{5/2}$ BE values for $Cu_2ZnSnSe_4$ and Cu_2Se[27] are in the same range and thus some of the Se 3d intensity could also be attributed to selenium being in a CZGSe kesterite or copper selenide environment – in particular considering the small but non-zero intensities of the (Ge 3d and) Cu 3p lines. The secondary contribution to the AG-CZGSe Se $3d_{5/2}$ line at higher BE is tentatively being ascribed to oxidized selenium, i.e.

an SeO_x – type species (with x<2). Note that the Se $3d_{5/2}$ line of SeO_2 can be found at much higher BE values[27], but as indicated by the respective BE range on top of Figure 2a the respective BEs for substoichiometric selenium oxides can legitimately be expected to be lower. However, based on the reported BE range for selenium or $GeSe_x$ compounds (see top of Figure 2a) also the presence of elemental selenium or $GeSe_x$ – type species at the surface of the AG-CZGSe absorber cannot be excluded.

The main Se 3d contribution of the E-CZGSe sample is ascribed to selenium in a kesterite environment (here CZGSe) and the secondary contribution is tentatively attributed to elemental selenium or a Ge-Se species (see reference BE position for GeSe and $GeSe_2$ at the top of Figure 2a and discussion in conjunction with **Figure 2b** below and detailed discussion in Supporting Information). The slightly higher BE of the Se $3d_{5/2}$ main contribution of the E-CZGSe spectrum compared to that reported for $Cu_2ZnSnSe_4$ can most likely be attributed to the higher bandgap of CZGSe.

For the EP-CZGSe sample, the Se 3d line can be fit by one contribution having the same $3d_{5/2}$ BE as the main Se $3d_{5/2}$ contribution of the E-CZGSe absorber and is thus being ascribed to selenium in a CZGSe environment.

The Ge 3d spin-orbit split spectra are shown in Figure 2b. Only the spectrum of the E-CZGSe absorber needs two doublets to reasonably fit the Ge 3d spectrum. The Ge $3d_{5/2}$ main contribution of the E-CZGSe sample as well as the respective lines of the AG-CZGSe and EP-CZGSe absorber are at a BE value of (30.7 ± 0.1) eV, which we – in agreement with the attribution (of the main contribution) of the Se 3d line – ascribe to Ge in a CZGSe environment. The secondary contribution to the Ge $3d_{5/2}$ line of the E-CZGSe absorber is found at lower BE: (30.4 ± 0.1) eV,

indicating that after HCl etching some of the Ge at the sample surface is present in an oxidation state lower than it would have in a CZGSe environment (i.e. < +4). The direct comparison with Ge $3d_{5/2}$ BE values for a Ge-Se – type species at the top of Figure 2b, suggests the formation of a substoichiometric Ge_xSe_y phase (in agreement with the attribution of the secondary Se 3d contribution above). However, based on the stated Ge $3d_{5/2}$ reference positions also the presence of elemental Ge cannot be excluded. The formation of elemental Ge and/or Ge-Se – type species on top of the CZGSe absorber upon HCl etching is also reasonable from a chemical point of view: While Zn-Se and Cu-Se (bonds) can be dissolved in acids, Ge-Se bonds and Ge are reasonable stable – even in concentrated acids.[36] In case the secondary Se 3d and Ge 3d components are the result of the presence of Ge-Se – type species also the apparent removal of this phase during the passivation treatment using $(NH_4)_2S$ can be understood from the chemistry perspective. We suggest a very simple Se-S ion-exchange based mechanism: $Ge_xSe_y + (NH_4)_2S \rightarrow Ge_xS_y + (NH_4)_2Se$ with Ge_xS_y being soluble in water (as being present in the ammonium sulfide solution as well as in the rinsing bath). However, despite the expected decrease of the Ge 3d line upon the passivation treatment (due to the removal of elemental Ge and/or a Ge-Se – type species) its intensity increases (see Figure S5 in Supporting Information). As a matter of fact, all photoemission lines increase upon the $(NH_4)_2S$ treatment. This can be explained by the removal

of significant amounts of C- and O-containing surface contaminants that were partially deposited on the sample upon the HCl etch treatment (see Figure S6 in Supporting Information).

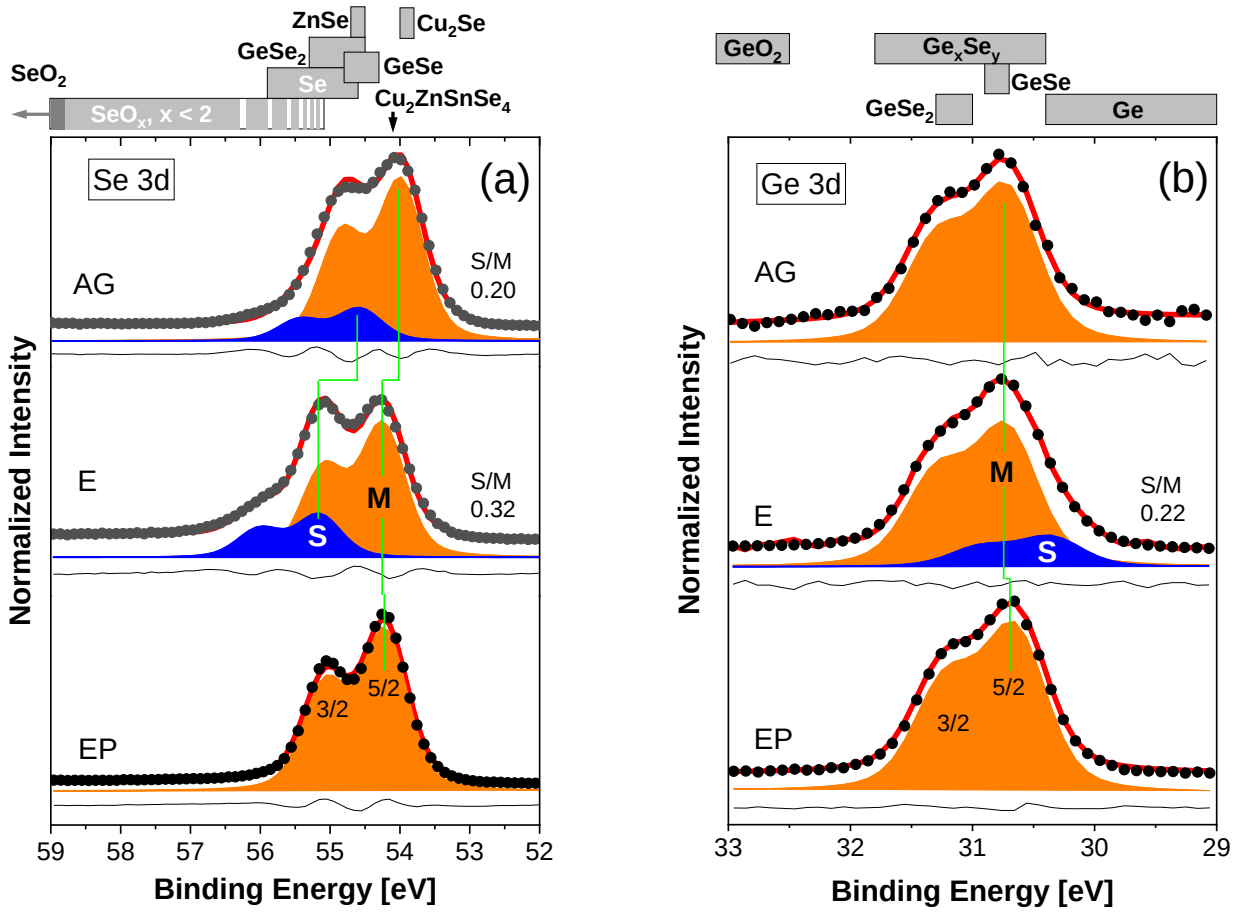

Figure 2. HAXPES detail spectra of the Se 3d (a) and Ge 3d (b) shallow core levels. The 3/2 and 5/2 components of the 3d lines are indicated for the main (M) contribution depicted in orange. The secondary (S) contribution required to appropriately describe the raw data (shown as dots) is depicted in blue. $3d_{5/2}$ reference BE positions from Ref.[27] for potentially formed compounds are shown on top of the panels.

In order to also reveal the impact of the different chemical treatments on the electronic (surface) structure of the CZGSe absorbers, the spectra of the valence band (VB) region (see **Figure 3**) are

consulted next. First, we compare the spectral shape of the spectra: While the spectra of the E- and EP-CZGSe absorbers are very similar, the spectrum of the AG-CZGSe sample looks quite different. To understand this spectral difference, we compare to computed total density of states (DOS) of ZnSe[37] and CZGSe[38] also depicted in Figure 3. For the spectrum of AG-CZGSe absorber, we find an excellent agreement with the DOS of ZnSe – in agreement with the chemical structure discussion above – and the spectra of the E- and EP-CZGSe samples resemble the DOS of CZGSe well. Note that the energy scale of the computed DOS was offset and expanded to best overlap with the spectral features of the measured spectra. To determine the position of the VBM with respect to E_F, we derive the intersection of the linear approximation of the leading VB spectrum edge and the background, as indicated by red lines in Figure 3. The derived VBM values for the AG-, E-, and EP-CZGSe absorbers are 0.53, 0.42, and 0.46 (± 0.10) eV. Considering the optical bulk bandgap of ZnSe (2.7 eV)[39] or CZGSe (1.4 eV as measured by EQE, see Figure S2 in Supporting Information), we find E_F closer to the VBM than to the conduction band minimum, indicating p-type conductivity at all sample surfaces. While this is expected for the CZGSe absorber, this is somewhat surprising for the (usually n-type) ZnSe covered CZGSe (AG-CZGSe sample). Explanations for this observation would be significant (upward) band bending inside the ZnSe (as a result of interface formation) or a non-negligible Cu 3d-derived contribution of underlying or not-covered CZGSe to the VBM region of the spectrum. In the latter two cases, the derived VBM would not be representative of the electronic structure of ZnSe but would rather need to be attributed to the VB of the CZGSe absorber.

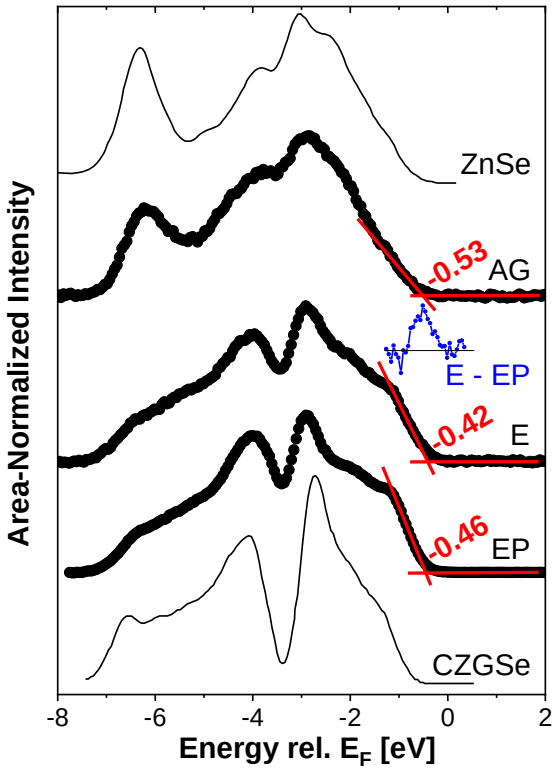

Figure 3. HAXPES spectra of the Valence band (VB) region

To reveal, why solar cells based on EP-CZGSe absorbers outperform their counterparts based on E-CZGSe, we closely inspect the VBM region of the respective spectra. We find a small difference in the spectral region of the VB onset: The 'foot' (i.e., the experimental data that deviates from the linear edge approximation around the intersection with the background) is more pronounced for the E-CZGSe spectrum compared to the spectrum of the EP-CZGSe absorber. This becomes very clear when computing the difference of the corresponding spectra (see "E-EP" in Figure 3); there is a significant higher spectral intensity around E_F in the spectrum of the E-CZGSe sample. An explanation could be spectral intensity that is related to the observed Se, Ge-Se, and/or Ge – type species formed during HCl-etching. Note that some of these compounds have a narrow

bandgap (in particular when germanium is in a low oxidation state). For p-type GeSe a bandgap of around 1.1 eV is reported[40] and thus the observed additional intensity around E_F could also be related to the VBM of that Ge-Se – type species. In any case, the presence/formation of a narrow bandgap layer at the emitter/absorber interface would certainly explain the losses observed for corresponding solar cell devices (see Figure 1 and related discussion above).

3.2. Solar cells heat treatment

Several reports on heat treatments of kesterite/CdS stacks or complete kesterite-based solar cells to promote chemical interaction at the interface and/or elemental interdiffusion can be found in literature.[41,42] Especially, Cu depletion and Cd incorporation into the uppermost region of the absorber and Zn incorporation into the buffer are discussed as beneficial effects.[43] Those modifications are likely to affect the energy level alignment at the kesterite/buffer interface as well as the concentration of free charge carriers on both sides of the heterojunction, ultimately determining interface recombination. Hence, controlled heat treatments (HTs) of kesterite solar cells can improve their optoelectronic characteristics resulting in higher V_{OC}, J_{SC}, and efficiency values, presumably due to a reduced charge carrier recombination at the interface.

First, we present the effects on the current-voltage characteristic (JV) and EQE of 60, 90 and 120min long 200°C-HTs performed on solar cells prepared from an EP-CZGSE absorber and a CdS buffer layer. Note that these devices had a 120 nm MgF_2 anti-reflection coating (ARC) layer. The V_{OC} increases while the FF decreases with HT duration (**Table 1**).

Table 1. Electrical parameters of solar cells prepared with EP absorbers and different HT durations

Buffer	Heat Treatment [min][a)]	V_{OC} [mV]	J_{SC} [mA.cm^{-2}] [b)]	FF [%]	η [%][b)]	R_S [Ω.cm^2]	R_{Sh} [Ω.cm^2]	E_U [meV]
CdS-previous record [c)]	none	558	22.8 [d)]	60	7.6[d)]			
CdS-this work[e)]	none	593	18.5	59.3	6.5	3.6	292	27
	60	625	24.4	55.7	8.5	4.4	248	31
	90	645	24.4	52.3	8.2	5.9	189	31
	120	663	23.8	48.9	7.7	6.3	187	37
ZnOS-This work [e)]	None	582	23.2	55.8	7.5	2.5	198	28
	240	663	14.8	36.7	3.6	17.7	110	35

[a)]Sum of heat treatments durations [b)] Total area [c)] Choubrac et al, one cell[17] [d)] Active area [e)]Evolution of the record cell

Additional experiments show that device aging at room temperature in ambient atmosphere - at the timescale of weeks - also manifests in improved V_{OC} and reduced FF but to a lower extent (see Supporting Information – Figure S7 for more details) and so the HT not only accelerates the aging effects but activates additional mechanisms. In the EQE of respective devices significant HT-induced changes can be observed (see **Figure 4**): first, a general EQE improvement is observed, which is consistent with the reduction of interfacial charge carrier recombination. Second, the absorption due to CdS in the 350-550 nm wavelength range is reduced. This is in agreement with reports suggesting that upon HT, Zn diffuses into the CdS buffer, converting the buffer material (partially) into a wider bandgap (Cd,Zn)S.[43,44] Third, HT induces an EQE increases in the wavelength regime between 550 and 870 nm, when its duration is limited to 90 min. For a HT time of 120 min the EQE decreases again in this wavelength regime.

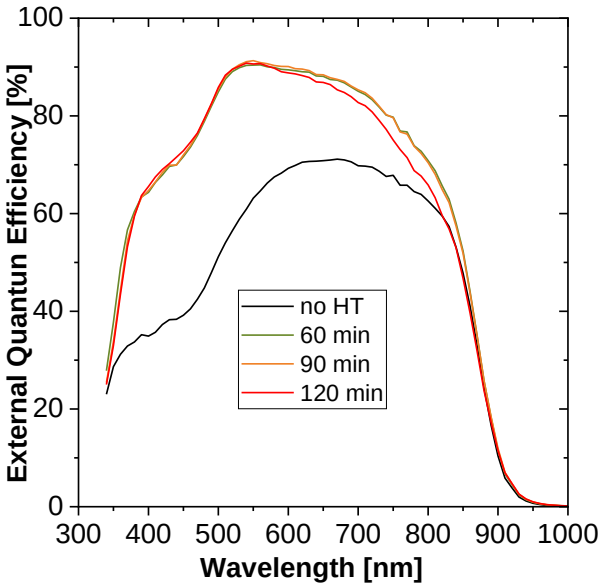

Figure 4. EQE spectra of solar cells prepared with EP absorber, CdS buffer layer and different HT durations

We attribute the EQE changes in this long wavelength region to changing charge carrier collection lengths, which can have various origins: Variation of the space charge region width (due to changes in the doping profile, changes on the grain boundaries and/or of the transport properties of the absorber (affecting the diffusion length of the charge carriers).

To summarize, the V_{OC} increases with HT duration, while FF slightly decreases, and J_{SC} reaches a maximum for HT times between 60 and 90 min. As a result, the highest power conversion efficiency of 8.5 % (total area, with ARC) is achieved for a 60 min HT. This represents the highest reported efficiency for solar cells based on pure germanium kesterite (CZGSe) absorbers. Compared to the previous record device (Table 1), achieved with the same absorber and buffer layer processes,[17] but without etching /passivation treatment or HT, V_{OC} and J_{SC} are significantly improved (+67 mV and +1.6 mA/cm², respectively) while FF is slightly decreased (-3 %).

Compared to state-of-the- art CZTSSe based[2] and mixed Sn/Ge kesterite CZTGSe[16] solar cells, the highest performance deficit can be observed for FF of the CZGSe cell (**Table 2**).

Table 2. Electrical parameters of the solar cells with highest efficiency and highest VOC reported in this article, and comparison with literature. According to Carron et al,[29] using b), c) or d) to measure E_g induces deviation in the range of 15 meV – as shown in Supplementary Information section 2.

Origin	Sample	V_{OC} [mV]	J_{SC} [mA.cm^{-2}][a)]	FF [%]	η [%][a)]	$V_{OC}/V_{OC,SQ}$	$J_{SC}/J_{SC,SQ}$	FF/FF_{SQ}	E_g [eV]	E_{RR} [eV]	E_U [meV]	Total Area [cm²]
This Work	CdS – 12h[k)]	739	17.3	55.2	7.1	65%	53%	62%	1.40[b)]	1.35[e)] 1.36[f)]	37	0.25
	CdS – 1h[k)]	625	24.4	55.7	8.5	55%	73%	62%	1.39[b)]	1.35[e)]	31	0.52
	ZnOS – 4h	663	14.8	36.7	3.6	58%	45%	41%	1.40[b)]	1.36[e)]	35	0.15
	ZnOS – no HT	582	23.2	55.8	7.5	51%	71%	62%	1.40[b)]	1.36[e)]	28	0.5
Litterature	Record CZTSSe[h), k)]	513	35.2	69.8	12.6	58%	81%	80%	1.13[c)]			0.42
	Record CZTGSe[i), k)]	527	32.2	72.7	12.3	61%	73%	84%	1.11[d)]	1.08[d)]	23	0.52
	Record CZTS[j), k)]	731	21.7	69.3	11.0	59%	75%	77%	1.5[d)]			0.23
	Previous record CZGSe[k)]	558	22.8[g)]	60	7.6[g)]	48%	72%	67%	1.43[c)]	1.36[e,f)]		0.5

[a)]Total area; [b)] From $(E.EQE)^2$ vs E; [c)] From EQE derivative; [d)] From $[E.\ln(1-EQE)]^2$ vs E; [e)] From EQE linear extrapolation; [f)] From PL_{Max}; [g)] Active area; [h)] Wang et al[2]; [i)]Kim et al[16]; [j)]Yan et al[43]; [j)] Choubrac et al[17]; [k)]With ARC

As the V_{OC} continues to increase even for durations up to 120 min (see Table 1), a new batch of CZGSe/CdS solar cells was prepared employing the optimization strategies discussed above, but with much extended HT duration (12h) with the goal to achieve the highest possible V_{OC}. This long annealing indeed led to a solar cell with a V_{OC} of 739 mV (Table 2, **Figure 5**). As the bandgap

energy of the absorber is E_g=1.40 eV, this open circuit voltage represented 65% of $V_{OC,SQ}$. To our knowledge, this value is (with respect to the corresponding theoretical limit) the highest reported open circuit voltage for any kesterite – based solar cell. As a matter of fact this $V_{OC}/V_{OC,SQ}$level is close to that of record $CuInSe_2$ solar cells, reaching 66% of $V_{OC,SQ}$.[45,46]

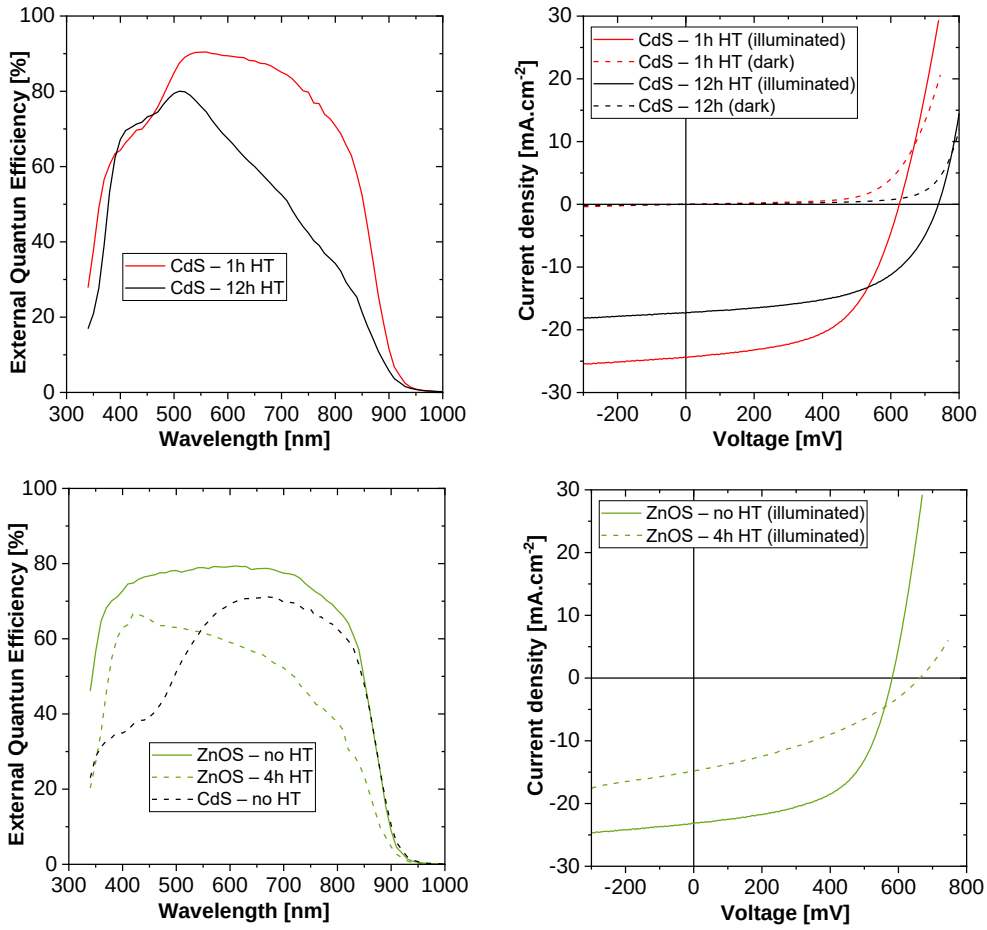

Figure 5. EQE(left) and J-V(right) curves of the solar cells with highest efficiency and highest V_{OC} reported in this article
Top: with CdS buffer layer, bottom: with ZnOS buffer layer

3.3. Zn(O,S,OH) Alternative buffer layer

A batch of solar cells based on EP-CZGSe were prepared using a CBD-Zn(O,S,OH) buffer (instead of the commonly used CBD-CdS buffer). Prior to annealing, the best cell shows a V_{OC} close to that measured for the CdS reference, while J_{SC} is higher but FF is reduced. A 240 min HT yields an improved V_{OC} of 663 mV. However, FF and collection length are degraded significantly (see Table1 and Figure 5). As a result, the highest efficiency for the CZGSe/Zn(O,S,OH) heterojunction of 7.5 % (total area, no ARC) is achieved without any HT. This represents the highest reported performance of any kesterite/Zn(O,S,OH) – based solar cell. The deteriorating effects associated to HT are similar but more pronounced in comparison to those observed with the identically prepared (EP) absorber and CdS buffer (see Figure S8, Supporting Information). In summary, the Zn(O,S,OH) buffer appears to be a very promising alternative to CdS for CZGSe solar cells as before HT it yields a higher efficiency than CdS (Table 1), and presents two significant advantages: Zn(O,S,OH) has a higher bandgap resulting in improved current collection in the UV wavelength region (lower absorption in the 300-550 nm range) and is free of toxic elements. While a similar V_{OC} gain is obtained during HT, the main limitation currently seems to be due to some (additional) detrimental effects during the annealing. Those effects could possibly be avoided (or mitigated) by designing new strategies after clarification of the HT-induced beneficial effects. HT or surface Cd-alloying/doping could be performed before Zn(O,S,OH) buffer deposition or Zn diffusion from the absorber to the buffer could be hindered by application of interfacial (chemical inert barrier/passivation) layers.

3.4. Impact of Sn by Ge substitution on performance and present limitations

Next, we will discuss the results with respect to reports in literature in order to shed light on the underlying mechanism of why the substitution of Sn by Ge increases V_{OC} and what factors might still limit the performance.

There are two main factors keeping V_{OC} far from theoretical optimum, namely the intrinsic properties of the absorber and the interface properties. In the literature on kesterite-based solar cells,[19] it is often suggested that the absorber/buffer interface is crucial in that respect. In particular, for S-rich CZTSSe – based solar cells a negative conduction band offset (CBO) at the absorber/CdS heterojunction is widely reported to be formed, being a potential factor that limits V_{OC}.[47] For S-poor or S-free kesterites mainly aligned conduction bands or positive CBOs, respectively, have been reported when employing CdS as buffer layer.[48,49] The latter CB configurations are likely not to increase interface recombination, however, too large (positive) CBOs might represent an energetic barrier for unimpeded carrier transport across the heterojunction. As the addition of Ge has a similar effect on the electronic structure of CZTSe compared to the addition of S, i.e. an increase in bandgap energy due to mainly an increase of the CB maximum,[50] a similar evolution of the energy level alignment at the CZTGSe/CdS interface can be expected, i.e. a low Ge-content results in a beneficial slightly positive or aligned CBO, while a high Ge-content may result in an aligned or negative CBO. Collord et al.[14] reported a clear drop of efficiency for Ge/(Ge+Sn) > 0.5, i.e. for kesterite absorbers with a bandgap > 1.3 eV, that they attributed to some extent to the formation of a detrimental negative CBO. Consistently, other works on wide bandgap kesterite absorbers reported a significant V_{OC} increase when employing alternative buffer layers in combination with high S and/or high Ge containing kesterite: (Zn,Cd)S[51] or (Zn,Sn)O on CZTS[52,53] and Zn(O,S) on CZGSSe[18]. These alternative n-type junction

partners are supposed to have a larger bandgap energy than CdS and a better-suited electronic structure (e.g., lower electron affinity) resulting in a more beneficial CB alignment with wide bandgap kesterites.

For the solar cell of highest V_{OC} (with CdS buffer and 12h HT), E_a and E_{RR} are measured to be 1.33 eV and 1.35 eV, respectively (see Table 2, and S2 and S9 in Supporting Information). The small deviation between those two values allows the conclusion that V_{OC} is not or very little limited by an increase recombination rate at the absorber/buffer interface. Therefore, the main V_{OC} limitation in this device must originate from intrinsic absorber properties, namely the presence of deep defects (that result in short charge carrier lifetimes and significant non-radiative recombination) and losses due to non-ideal absorption.[3,54,55] These absorption losses can be qualitatively assessed via the energy difference between bandgap and PL_{max} at room temperature - here 40meV (see Table 2 and S10 in Supporting Information), a moderate value but not an improvement compared to literature.[56] In detail, these losses are known to have two origins in kesterite: bandtailing and bandgap distribution. The bandtailing - as estimated via EQE - is here 37 meV which is again a low but not below standards value.[15] Thus, the highest obtained V_{OC} remains slightly limited by losses related to non-ideal absorption, at least in part due to the presence of bandtailing.

As the interface and absorption losses (respectively correlated to the differences E_{RR}-E_a and E_g-E_{PLmax}) are not smaller than those reported for kesterite solar cells, the increase in $V_{OC}/V_{OC,SQ}$ reported here can be attributed to improvement related to the deep defect (its concentration, capture cross section and/or deepness) when Sn is completely substituted by Ge.

4. Conclusion

To evaluate the full potential of substituting Sn by Ge in kesterite-based solar cells different strategies have been implemented to improve the CZGSe/buffer heterojunction:

1- It has been shown that only a combination of different surface treatments (etching in hot HCl and passivation in aqueous $(NH_4)_2S$ solution) is able to remove all undesired and detrimental secondary phases. Detailed analysis of the treated CZGSe surface by HAXPES reveals that HCl efficiently removes ZnSe, but leaves behind a narrow bandgap species best described by elemental Ge and/or Ge-Se – type compound. This species is only removed in the second $(NH_4)_2S$ treatment.

2- A heat treatment has been established that results in a record performance for Sn-free kesterite solar cells: 8.5% total area efficiency (with ARC).

3- Application of an alternative buffer layer, namely Zn(O,S,OH) instead of CdS has successfully been realized. A record performance for any kesterite solar cell with a Zn(O,S,OH) buffer has been achieved: 7.5% total area efficiency (without ARC).

More important: we clearly confirm the emerging trend that Ge for Sn substitution is a successful strategy to improve the V_{OC} of kesterite solar cells, which is considered to be the main limitation of the technology. In particular, a kesterite solar cell with a $V_{OC}/V_{OC,SQ}$ ratio of 65% has been achieved, compared to 58% for the Ge-free record device. A direct transfer of this V_{OC} gain to current state-of-the-art devices suggests that Ge for Sn substitution could push the kesterite solar cell efficiency higher than 14%.

ASSOCIATED CONTENT

Supporting Information. Supporting_Information.pdf contains the following 9 sections:

SI - 1: Effect of annealing on absorber bandgap

SI – 2: Comparison of different methods for bandgap extraction from EQE

SI – 3: Effect of the etching and passivation on Photoluminescence on absorbers

SI – 4: HAXPES shallow core level spectra

SI – 5: C 1s and O 1s HAXPES detail spectra

SI – 6: Aging effect on VOC and FF

SI – 7: Comparison of the effect of annealing on AG-CZGSe/CdS and EP-CZGSe/Zn(S,O,OH) solar cells

SI – 8: VOC vs T of high VOC solar cell

SI – 9: Photoluminescence on highest VOC solar cell

AUTHOR INFORMATION

Corresponding Author

*Choubrac Leo, leo.choubrac@helmholtz-berlin.de, leo.choubrac@gmail.com

Funding Sources

This project has received funding from the European Union's Horizon 2020 Research and Innovation Program under grant agreement No. 640868.

REFERENCES

(1) Giraldo, S.; Jehl, Z.; Placidi, M.; Izquierdo-Roca, V.; Pérez-Rodríguez, A.; Saucedo, E. Progress and Perspectives of Thin Film Kesterite Photovoltaic Technology: A Critical Review. *Adv. Mater.* **2019**, *31* (16), 1806692. https://doi.org/10.1002/adma.201806692.

(2) Wang, W.; Winkler, M. T.; Gunawan, O.; Gokmen, T.; Todorov, T. K.; Zhu, Y.; Mitzi, D. B. Device Characteristics of CZTSSe Thin-Film Solar Cells with 12.6% Efficiency. *Adv. Energy Mater.* **2014**, *4* (7), 1301465. https://doi.org/10.1002/aenm.201301465.

(3) Romanyuk, Y. E.; Haass, S. G.; Giraldo, S.; Placidi, M.; Tiwari, D.; Fermin, D. J.; Hao, X.; Xin, H.; Schnabel, T.; Kauk-Kuusik, M.; Pistor, P.; Lie, S.; Wong, L. H. Doping and Alloying of Kesterites. *J. Phys. Energy* **2019**, *1* (4), 044004. https://doi.org/10.1088/2515-7655/ab23bc.

(4) Li, J.; Wang, D.; Li, X.; Zeng, Y.; Zhang, Y. Cation Substitution in Earth-Abundant Kesterite Photovoltaic Materials. *Adv. Sci.* **2018**, *5* (4), 1700744. https://doi.org/10.1002/advs.201700744.

(5) Shockley, W.; Queisser, H. J. Detailed Balance Limit of Efficiency of P-n Junction Solar Cells. *J. Appl. Phys.* **1961**, *32* (3), 510–519. https://doi.org/10.1063/1.1736034.

(6) Bourdais, S.; Choné, C.; Delatouche, B.; Jacob, A.; Larramona, G.; Moisan, C.; Lafond, A.; Donatini, F.; Rey, G.; Siebentritt, S.; Walsh, A.; Dennler, G. Is the Cu/Zn Disorder the Main Culprit for the Voltage Deficit in Kesterite Solar Cells? *Adv. Energy Mater.* **2016**, *6* (12), 1502276. https://doi.org/10.1002/aenm.201502276.

(7) Grenet, L.; Suzon, M. A. A.; Emieux, F.; Roux, F. Analysis of Failure Modes in Kesterite Solar Cells. *ACS Appl. Energy Mater.* **2018**, *1* (5), 2103–2113. https://doi.org/10.1021/acsaem.8b00194.

(8) Xin, H.; Vorpahl, S. M.; Collord, A. D.; Braly, I. L.; Uhl, A. R.; Krueger, B. W.; Ginger, D. S.; Hillhouse, H. W. Lithium-Doping Inverts the Nanoscale Electric Field at the Grain Boundaries in Cu2ZnSn(S,Se)4 and Increases Photovoltaic Efficiency. *Phys. Chem. Chem. Phys.* **2015**, *17* (37), 23859–23866. https://doi.org/10.1039/C5CP04707B.

(9) Gershon, T.; Sardashti, K.; Lee, Y. S.; Gunawan, O.; Singh, S.; Bishop, D.; Kummel, A. C.; Haight, R. Compositional Effects in Ag2ZnSnSe4 Thin Films and Photovoltaic Devices. *Acta Mater.* **2017**, *126*, 383–388. https://doi.org/10.1016/j.actamat.2017.01.003.

(10) Yan, C.; Sun, K.; Huang, J.; Johnston, S.; Liu, F.; Veettil, B. P.; Sun, K.; Pu, A.; Zhou, F.; Stride, J. A.; Green, M. A.; Hao, X. Beyond 11% Efficient Sulfide Kesterite Cu2ZnxCd1–XSnS4 Solar Cell: Effects of Cadmium Alloying. *ACS Energy Lett.* **2017**, *2* (4), 930–936. https://doi.org/10.1021/acsenergylett.7b00129.

(11) Shin, D.; Zhu, T.; Huang, X.; Gunawan, O.; Blum, V.; Mitzi, D. B. Earth-Abundant Chalcogenide Photovoltaic Devices with over 5% Efficiency Based on a Cu2BaSn(S,Se)4 Absorber. *Adv. Mater.* **2017**, *29* (24), 1606945. https://doi.org/10.1002/adma.201606945.

(12) Ghosh, A.; Chaudhary, D. K.; Biswas, A.; Thangavel, R.; Udayabhanu, G. Solution-Processed Cu2XSnS4 (X = Fe, Co, Ni) Photo-Electrochemical and Thin Film Solar Cells on Vertically Grown ZnO Nanorod Arrays. *RSC Adv.* **2016**, *6* (116), 115204–115212. https://doi.org/10.1039/C6RA24149B.

(13) Li, X.; Hou, Z.; Gao, S.; Zeng, Y.; Ao, J.; Zhou, Z.; Da, B.; Liu, W.; Sun, Y.; Zhang, Y. Efficient Optimization of the Performance of Mn2+-Doped Kesterite Solar Cell: Machine Learning Aided Synthesis of High Efficient Cu2(Mn,Zn)Sn(S,Se)4 Solar Cells. *Sol. RRL* **2018**, *2* (12), 1800198. https://doi.org/10.1002/solr.201800198.

(14) Collord, A. D.; Hillhouse, H. W. Germanium Alloyed Kesterite Solar Cells with Low Voltage Deficits. *Chem. Mater.* **2016**, *28* (7), 2067–2073. https://doi.org/10.1021/acs.chemmater.5b04806.
(15) Kim, S.; Kim, K. M.; Tampo, H.; Shibata, H.; Matsubara, K.; Niki, S. Ge-Incorporated Cu2ZnSnSe4 Thin-Film Solar Cells with Efficiency Greater than 10%. *Sol. Energy Mater. Sol. Cells* **2016**, *144*, 488–492. https://doi.org/10.1016/j.solmat.2015.09.039.
(16) Kim, S.; Kim, K. M.; Tampo, H.; Shibata, H.; Niki, S. Improvement of Voltage Deficit of Ge-Incorporated Kesterite Solar Cell with 12.3% Conversion Efficiency. *Appl. Phys. Express* **2016**, *9* (10), 102301. https://doi.org/10.7567/APEX.9.102301.
(17) Choubrac, L.; Brammertz, G.; Barreau, N.; Arzel, L.; Harel, S.; Meuris, M.; Vermang, B. 7.6% CZGSe Solar Cells Thanks to Optimized CdS Chemical Bath Deposition. *Phys. Status Solidi A* **2018**, *215* (13), 1800043. https://doi.org/10.1002/pssa.201800043.
(18) Schnabel, T.; Seboui, M.; Bauer, A.; Choubrac, L.; Arzel, L.; Harel, S.; Barreau, N.; Ahlswede, E. Evaluation of Different Buffer Materials for Solar Cells with Wide-Gap Cu 2 ZnGeS x Se 4−x Absorbers. *RSC Adv.* **2017**, *7* (64), 40105–40110. https://doi.org/10.1039/C7RA06438A.
(19) Platzer-Björkman, C.; Barreau, N.; Bär, M.; Choubrac, L.; Grenet, L.; Heo, J.; Kubart, T.; Mittiga, A.; Sanchez, Y.; Scragg, J.; Sinha, S.; Valentini, M. Back and Front Contacts in Kesterite Solar Cells: State-of-the-Art and Open Questions. *J. Phys. Energy* **2019**, *1* (4), 044005. https://doi.org/10.1088/2515-7655/ab3708.
(20) Brammertz, G.; Kohl, T.; De Wild, J.; Meuris, M.; Vermang, B.; Poortmans, J. Crystallization Properties of Cu2ZnGeSe4. *Thin Solid Films* **2019**, *670*, 76–79. https://doi.org/10.1016/j.tsf.2018.12.015.
(21) Vermang, B.; Brammertz, G.; Meuris, M.; Schnabel, T.; Ahlswede, E.; Choubrac, L.; Harel, S.; Cardinaud, C.; Arzel, L.; Barreau, N.; Deelen, J. van; Bolt, P.-J.; Bras, P.; Ren, Y.; Jaremalm, E.; Khelifi, S.; Yang, S.; Lauwaert, J.; Batuk, M.; Hadermann, J.; Kozina, X.; Handick, E.; Hartmann, C.; Gerlach, D.; Matsuda, A.; Ueda, S.; Chikyow, T.; Félix, R.; Zhang, Y.; G. Wilks, R.; Bär, M. Wide Band Gap Kesterite Absorbers for Thin Film Solar Cells: Potential and Challenges for Their Deployment in Tandem Devices. *Sustain. Energy Fuels* **2019**, *3* (9), 2246–2259. https://doi.org/10.1039/C9SE00266A.
(22) Troviano, M.; Taretto, K. Temperature-Dependent Quantum Efficiency Analysis of Graded-Gap Cu(In,Ga)Se2 Solar Cells. *Sol. Energy Mater. Sol. Cells* **2011**, *95* (11), 3081–3086. https://doi.org/10.1016/j.solmat.2011.06.038.
(23) Scragg, J. J. S.; Choubrac, L.; Lafond, A.; Ericson, T.; Platzer-Björkman, C. A Low-Temperature Order-Disorder Transition in Cu2ZnSnS4 Thin Films. *Appl. Phys. Lett.* **2014**, *104* (4), 041911. https://doi.org/10.1063/1.4863685.
(24) Rey, G.; Redinger, A.; Sendler, J.; Weiss, T. P.; Thevenin, M.; Guennou, M.; El Adib, B.; Siebentritt, S. The Band Gap of Cu2ZnSnSe4: Effect of Order-Disorder. *Appl. Phys. Lett.* **2014**, *105* (11), 112106. https://doi.org/10.1063/1.4896315.
(25) Gorgoi, M.; Svensson, S.; Schäfers, F.; Öhrwall, G.; Mertin, M.; Bressler, P.; Karis, O.; Siegbahn, H.; Sandell, A.; Rensmo, H.; Doherty, W.; Jung, C.; Braun, W.; Eberhardt, W. The High Kinetic Energy Photoelectron Spectroscopy Facility at BESSY Progress and First Results. *Nucl. Instrum. Methods Phys. Res. Sect. Accel. Spectrometers Detect. Assoc. Equip.* **2009**, *601* (1), 48–53. https://doi.org/10.1016/j.nima.2008.12.244.

(26) Schaefers, F.; Mertin, M.; Gorgoi, M. KMC-1: A High Resolution and High Flux Soft x-Ray Beamline at BESSY. *Rev. Sci. Instrum.* **2007**, *78* (12), 123102. https://doi.org/10.1063/1.2808334.
(27) Naumkin, A. V.; Kraut-Vass, A.; Powell, C. J.; National Institute of Standards and Technology (U.S.). *NIST X-Ray Photoelectron Spectroscopy Database*; Distributed by the Measurement Services Division of the National Institute of Standards and Technology (NIST) Technology Services: Gaithersburg, MD, 2008.
(28) Rühle, S. Tabulated Values of the Shockley–Queisser Limit for Single Junction Solar Cells. *Sol. Energy* **2016**, *130*, 139–147. https://doi.org/10.1016/j.solener.2016.02.015.
(29) Carron, R.; Andres, C.; Avancini, E.; Feurer, T.; Nishiwaki, S.; Pisoni, S.; Fu, F.; Lingg, M.; Romanyuk, Y. E.; Buecheler, S.; Tiwari, A. N. Bandgap of Thin Film Solar Cell Absorbers: A Comparison of Various Determination Methods. *Thin Solid Films* **2019**, *669*, 482–486. https://doi.org/10.1016/j.tsf.2018.11.017.
(30) Scheer, R.; Schock, H.-W. *Chalcogenide Photovoltaics: Physics, Technologies, and Thin Film Devices*; John Wiley & Sons, 2011.
(31) Siebentritt, S.; Rey, G.; Finger, A.; Regesch, D.; Sendler, J.; Weiss, T. P.; Bertram, T. What Is the Bandgap of Kesterite? *Sol. Energy Mater. Sol. Cells* **2016**, *158*, 126–129. https://doi.org/10.1016/j.solmat.2015.10.017.
(32) Timmo, K.; Altosaar, M.; Raudoja, J.; Grossberg, M.; Danilson, M.; Volobujeva, O.; Mellikov, E. Chemical Etching of Cu2ZnSn(S,Se)4 Monograin Powder. In *2010 35th IEEE Photovoltaic Specialists Conference*; 2010; pp 001982–001985. https://doi.org/10.1109/PVSC.2010.5616411.
(33) Buffière, M.; Brammertz, G.; El Mel, A.-A.; Barreau, N.; Meuris, M.; Poortmans, J. Effect of Ammonium Sulfide Treatments on the Surface Properties of Cu2ZnSnSe4 Thin Films. *Thin Solid Films* **2017**, *633*, 135–140. https://doi.org/10.1016/j.tsf.2016.09.011.
(34) Bessolov, V. N.; Lebedev, M. V.; Rud', V. Yu.; Rud', Yu. V. Photoluminescence of II–IV–V2 and I–III–VI2 Crystals Passivated in a Sulfide Solution. *Tech. Phys. Lett.* **1998**, *24* (11), 875–876. https://doi.org/10.1134/1.1262298.
(35) Redinger, A.; Unold, T. High Surface Recombination Velocity Limits Quasi-Fermi Level Splitting in Kesterite Absorbers. *Sci. Rep.* **2018**, *8* (1), 1–9. https://doi.org/10.1038/s41598-018-19798-w.
(36) Rumble, J. CRC Handbook of Chemistry and Physics, 100th Edition https://www.crcpress.com/CRC-Handbook-of-Chemistry-and-Physics-100th-Edition/Rumble/p/book/9781138367296(37) Bosco, J. P.; Scanlon, D. O.; Watson, G. W.; Lewis, N. S.; Atwater, H. A. Energy-Band Alignment of II-VI/Zn3P2 Heterojunctions from x-Ray Photoemission Spectroscopy. *J. Appl. Phys.* **2013**, *113* (20), 203705. https://doi.org/10.1063/1.4807646.
(38) Chen, D.; Ravindra, N. M. Electronic and Optical Properties of Cu2ZnGeX4 (X=S, Se and Te) Quaternary Semiconductors. *J. Alloys Compd.* **2013**, *579*, 468–472. https://doi.org/10.1016/j.jallcom.2013.06.048.
(39) López-Marino, S.; Sánchez, Y.; Placidi, M.; Fairbrother, A.; Espindola-Rodríguez, M.; Fontané, X.; Izquierdo-Roca, V.; López-García, J.; Calvo-Barrio, L.; Pérez-Rodríguez, A.; Saucedo, E. ZnSe Etching of Zn-Rich Cu2ZnSnSe4: An Oxidation Route for Improved Solar-Cell Efficiency. *Chem. – Eur. J.* **2013**, *19* (44), 14814–14822. https://doi.org/10.1002/chem.201302589.

(40) Liu, S.-C.; Mi, Y.; Xue, D.-J.; Chen, Y.-X.; He, C.; Liu, X.; Hu, J.-S.; Wan, L.-J. Investigation of Physical and Electronic Properties of GeSe for Photovoltaic Applications. *Adv. Electron. Mater.* **2017**, *3* (11), 1700141. https://doi.org/10.1002/aelm.201700141.

(41) Neuschitzer, M.; Sanchez, Y.; Olar, T.; Thersleff, T.; Lopez-Marino, S.; Oliva, F.; Espindola-Rodriguez, M.; Xie, H.; Placidi, M.; Izquierdo-Roca, V.; Lauermann, I.; Leifer, K.; Pérez-Rodriguez, A.; Saucedo, E. Complex Surface Chemistry of Kesterites: Cu/Zn Reordering after Low Temperature Postdeposition Annealing and Its Role in High Performance Devices. *Chem. Mater.* **2015**, *27* (15), 5279–5287. https://doi.org/10.1021/acs.chemmater.5b01473.

(42) Xie, H.; López-Marino, S.; Olar, T.; Sánchez, Y.; Neuschitzer, M.; Oliva, F.; Giraldo, S.; Izquierdo-Roca, V.; Lauermann, I.; Pérez-Rodríguez, A.; Saucedo, E. Impact of Na Dynamics at the Cu2ZnSn(S,Se)4/CdS Interface During Post Low Temperature Treatment of Absorbers. *ACS Appl. Mater. Interfaces* **2016**, *8* (7), 5017–5024. https://doi.org/10.1021/acsami.5b12243.

(43) Yan, C.; Huang, J.; Sun, K.; Johnston, S.; Zhang, Y.; Sun, H.; Pu, A.; He, M.; Liu, F.; Eder, K.; Yang, L.; Cairney, J. M.; Ekins-Daukes, N. J.; Hameiri, Z.; Stride, J. A.; Chen, S.; Green, M. A.; Hao, X. Cu 2 ZnSnS 4 Solar Cells with over 10% Power Conversion Efficiency Enabled by Heterojunction Heat Treatment. *Nat. Energy* **2018**, *3* (9), 764–772. https://doi.org/10.1038/s41560-018-0206-0.

(44) Dimitrievska, M.; Giraldo, S.; Pistor, P.; Saucedo, E.; Pérez-Rodríguez, A.; Izquierdo-Roca, V. Raman Scattering Analysis of the Surface Chemistry of Kesterites: Impact of Post-Deposition Annealing and Cu/Zn Reordering on Solar Cell Performance. *Sol. Energy Mater. Sol. Cells* **2016**, *157*, 462–467. https://doi.org/10.1016/j.solmat.2016.07.009.

(45) Jehad AbuShama; Noufi, R.; Johnston, S.; Ward, S.; Wu, X. Improved Performance in CuInSe/Sub 2/ and Surface-Modified CuGaSe/Sub 2/ Solar Cells. In *Conference Record of the Thirty-first IEEE Photovoltaic Specialists Conference, 2005.*; 2005; pp 299–302. https://doi.org/10.1109/PVSC.2005.1488128.

(46) Feurer, T.; Bissig, B.; Weiss, T. P.; Carron, R.; Avancini, E.; Löckinger, J.; Buecheler, S.; Tiwari, A. N. Single-Graded CIGS with Narrow Bandgap for Tandem Solar Cells. *Sci. Technol. Adv. Mater.* **2018**, *19* (1), 263–270. https://doi.org/10.1080/14686996.2018.1444317.

(47) Bär, M.; Schubert, B.-A.; Marsen, B.; Wilks, R. G.; Pookpanratana, S.; Blum, M.; Krause, S.; Unold, T.; Yang, W.; Weinhardt, L.; Heske, C.; Schock, H.-W. Cliff-like Conduction Band Offset and KCN-Induced Recombination Barrier Enhancement at the CdS/Cu2ZnSnS4 Thin-Film Solar Cell Heterojunction. *Appl. Phys. Lett.* **2011**, *99* (22), 222105. https://doi.org/10.1063/1.3663327.

(48) Santoni, A.; Biccari, F.; Malerba, C.; Valentini, M.; Chierchia, R.; Mittiga, A. Valence Band Offset at the CdS/Cu2ZnSnS4 Interface Probed by x-Ray Photoelectron Spectroscopy. *J. Phys. Appl. Phys.* **2013**, *46* (17), 175101. https://doi.org/10.1088/0022-3727/46/17/175101.

(49) Minemoto, T.; Matsui, T.; Takakura, H.; Hamakawa, Y.; Negami, T.; Hashimoto, Y.; Uenoyama, T.; Kitagawa, M. Theoretical Analysis of the Effect of Conduction Band Offset of Window/CIS Layers on Performance of CIS Solar Cells Using Device Simulation. *Sol. Energy Mater. Sol. Cells* **2001**, *67* (1), 83–88. https://doi.org/10.1016/S0927-0248(00)00266-X.

(50) Chen, S.; Walsh, A.; Yang, J.-H.; Gong, X. G.; Sun, L.; Yang, P.-X.; Chu, J.-H.; Wei, S.-H. Compositional Dependence of Structural and Electronic Properties of

Cu${}_{2}$ZnSn(S,Se)${}_{4}$ Alloys for Thin Film Solar Cells. *Phys. Rev. B* **2011**, *83* (12), 125201. https://doi.org/10.1103/PhysRevB.83.125201.

(51) Sun, K.; Yan, C.; Liu, F.; Huang, J.; Zhou, F.; Stride, J. A.; Green, M.; Hao, X. Over 9% Efficient Kesterite Cu2ZnSnS4 Solar Cell Fabricated by Using Zn1–XCdxS Buffer Layer. *Adv. Energy Mater.* **2016**, *6* (12), 1600046. https://doi.org/10.1002/aenm.201600046.

(52) Ericson, T.; Larsson, F.; Törndahl, T.; Frisk, C.; Larsen, J.; Kosyak, V.; Hägglund, C.; Li, S.; Platzer-Björkman, C. Zinc-Tin-Oxide Buffer Layer and Low Temperature Post Annealing Resulting in a 9.0% Efficient Cd-Free Cu2ZnSnS4 Solar Cell. *Sol. RRL* **2017**, *1* (5), 1700001. https://doi.org/10.1002/solr.201700001.

(53) Cui, X.; Sun, K.; Huang, J.; Lee, C.-Y.; Yan, C.; Sun, H.; Zhang, Y.; Liu, F.; Hossain, Md. A.; Zakaria, Y.; Wong, L. H.; Green, M.; Hoex, B.; Hao, X. Enhanced Heterojunction Interface Quality To Achieve 9.3% Efficient Cd-Free Cu2ZnSnS4 Solar Cells Using Atomic Layer Deposition ZnSnO Buffer Layer. *Chem. Mater.* **2018**, *30* (21), 7860–7871. https://doi.org/10.1021/acs.chemmater.8b03398.

(54) Grossberg, M.; Krustok, J.; Hages, C. J.; Bishop, D. M.; Gunawan, O.; Scheer, R.; Lyam, S. M.; Hempel, H.; Levcenco, S.; Unold, T. The Electrical and Optical Properties of Kesterites. *J. Phys. Energy* **2019**, *1* (4), 044002. https://doi.org/10.1088/2515-7655/ab29a0.

(55) Hood, S. N.; Walsh, A.; Persson, C.; Iordanidou, K.; Huang, D.; Kumar, M.; Jehl, Z.; Courel, M.; Lauwaert, J.; Lee, S. Status of Materials and Device Modelling for Kesterite Solar Cells. *J. Phys. Energy* **2019**, *1* (4), 042004. https://doi.org/10.1088/2515-7655/ab2dda.

(56) Lee, Y. S.; Gershon, T.; Gunawan, O.; Todorov, T. K.; Gokmen, T.; Virgus, Y.; Guha, S. Cu2ZnSnSe4 Thin-Film Solar Cells by Thermal Co-Evaporation with 11.6% Efficiency and Improved Minority Carrier Diffusion Length. *Adv. Energy Mater.* **2015**, *5* (7), 1401372. https://doi.org/10.1002/aenm.201401372.

For Table of Contents use only